NUMERICAL STUDY OF AFTEREFFECTS OF OFFSHORE GENERATED FREAK WAVES SHOALING TO COAST

Hiroaki Kashima[1], Katsuya Hirayama[2], Nobuhito Mori[3]

Abstract

Nonlinear four-wave interactions influence the statistical properties of deep-water extreme waves such as a freak wave. However, the characteristics of deep-water generated freak wave shoaling to shallow water region are still not clearly understood. In this study, the numerical simulations using the Boussinesq model are conducted to investigate the aftereffects of the third-order nonlinear interactions from deep to shallow water region related to freak wave occurrences. It is possible to understand the characteristics of freak wave occurrence in the shallow water region using the Boussinesq model data, if appropriate higher-order nonlinear correction is considered analytically.

Key words: Third- nonlinear interactions, Boussinesq model, kurtosis, skewness, freak wave

1. Introduction

In the past two decades, the deep-water extreme waves such as a freak wave measured and caused several severe damages to offshore structures and vessels. An accurate estimation of maximum wave height and prediction of freak wave occurrence frequency is important for marine safety and ocean development. According to several studies on freak waves in deep-water, a kurtosis of the surface elevation which is indicator of the third-order nonlinear interactions (quasi-resonant four-wave interactions) can be related with a significant enhancement of freak wave occurrence (*e.g.* Yasuda and Mori, 1993). Janssen (2003) theoretically investigated the freak wave occurrence caused by a consequence of non-resonant four-wave interactions. He also found that the non-resonant nonlinear transfer is associated with the increase of fourth-order cumulant which is equivalent to kurtosis. In addition, he introduced the Benjamin-Feir Index to investigate the ratio of the nonlinearity to frequency dispersion for the narrow-banded unidirectional waves. Furthermore, the analytical relationship between the kurtosis, the maximum wave height and the occurrence probability of freak waves has been discussed in Mori and Janssen (2006). For a given nonlinearity of kurtosis, μ_4, the maximum wave height follows

$$p_m\left(H_{\max}\right)=\frac{N}{4}H_{\max}\exp^{\frac{-H_{\max}^2}{8}}\left[1+\left(\mu_4-3\right)A_H\left(H_{\max}\right)\right] \times\exp\left\{-N\exp^{\frac{-H_{\max}^2}{8}}\left[1+\left(\mu_4-3\right)B_H\left(H_{\max}\right)\right]\right\} \quad (1)$$

where p_{m} is the probability density function of the maximum wave height, $H_{\max}$. N is the number of waves corresponding to the storm duration. A_H and B_H are polynomials of $H_{\max}$ (Mori and Janssen, 2006). For μ_4 = 3, the results are identical to the ones following from the Rayleigh distribution. This frame work on the estimation of freak wave, named as MJ2006 here, was verified by the several wave flume experiments for unidirectional deep-water waves including the spatial development of the kurtosis, the wave height distribution and the probability density function of the maximum wave height in detail (*e.g.* Mori et al., 2007 and Petrova and Guedes Soares, 2009). Moreover, the recent work reported that directional dispersion reduces the enhancement of extreme wave generation due to the third-order nonlinear interactions (Waseda

[1]Port and Airport Research Institute, 3-1-1 Nagase, Yokosuka, Kanagawa 239-0826, Japan. kashima@pari.go.jp
[2]Port and Airport Research Institute, 3-1-1 Nagase, Yokosuka, Kanagawa 239-0826, Japan. hirayama@pari.go.jp
[3]Disaster Prevention Research Institute, Kyoto University, Gokasho, Uji, Kyoto 611-0011, Japan. mori@oceanwave.jp

et al., 2009). Several proposed a new formula for the kurtosis including the directional dispersion effects (*e.g.* Mori et al., 2011 and Xiao et al. 2013).

Although the characteristics of freak wave occurrence and its prediction in the deep water region become getting clear, there are a few studies about the characteristics of freak wave propagating from deep to shallow water region (*e.g.* Janssen and Onorato, 2007; Zeng and Trulsen, 2012; Trulsen et al., 2012). It is well known that the dependence of the kurtosis on four-wave interactions weakens in the shallow water region, if water depth h normalized by wave number k_p for deep-water waves, k_ph, is shallower than 1.363 (*e.g.* Yuen and Lake, 1982). However, based on the experimental results, Kashima et al. (2012) suggested that the aftereffects of the third-order nonlinear interactions from deep to shallow water region remains remarkable influences on random wave height distribution on the slope bathymetry.

Generally, a numerical simulation using the Boussinesq model has been widely used to estimate wave transformations in the shallow water region (Hirayama, 2002). The Boussinesq model shows high-level performance in the design of coast and harbor structures in Japan (*e.g.* Hirayama, 2013a). However, it is difficult to describe the freak wave occurrence in deep to shallow water region by the Boussinesq model because it can express only up to the second-order nonlinear interactions in the shallow water region. Thus, there is a gap of governing equation between deep and shallow water region from the extreme wave modeling point of view. It is necessary to investigate the aftereffects of generated freak waves by the third-order nonlinear interactions in deep water and their propagation to shallow water region on the slope using the Boussinesq model.

The purpose of this study is to understand the applicable range of the Boussinesq model for the aftereffects of the third-order nonlinear interactions from deep to shallow water region and relation to freak wave occurrences. First, the nonlinear statistical wave properties related to freak wave occurrences by the Boussinesq model are investigated through the comparison with the experimental data. Second, to be able to estimate the probability density function of maximum wave height as freak wave occurrences in shallow water region using the Boussinesq model results, the parameterization of nonlinear effects is proposed.

2. Numerical simulation

2.1 Numerical method

A series of numerical simulation, named NOWT-PARI originally developed by Hirayama (2002), was conducted to understand the nonlinear effects in the shallow water region. This simulation is based on the standard Boussinesq equations with improved dispersion characteristics as reported by Madsen and Sørensen (1992). The fundamental equations of continuity and momentum for x and y directions can be expressed as follows:

$$\frac{\partial \eta}{\partial t}+\frac{\partial P}{\partial x}+\frac{\partial Q}{\partial y}=0 \tag{2}$$

$$\begin{aligned}&\frac{\partial P}{\partial t}+gD\frac{\partial \eta}{\partial x}+\varepsilon\left[\frac{\partial}{\partial x}\left(\frac{P^2}{D}\right)+\frac{\partial}{\partial y}\left(\frac{PQ}{D}\right)\right]\\&=\mu^2\left[\begin{array}{l}\left(B+\frac{1}{3}\right)h^2\left(\frac{\partial^3 P}{\partial x^2\partial t}+\frac{\partial^3 Q}{\partial x\partial y\partial t}\right)+Bgh^3\left(\frac{\partial^3 \eta}{\partial x^3}+\frac{\partial^3 \eta}{\partial x\partial y^2}\right)\\+h\frac{\partial h}{\partial y}\left(\frac{1}{6}\frac{\partial^2 Q}{\partial x\partial t}+Bgh\frac{\partial^2 \eta}{\partial x\partial y}\right)+h\frac{\partial h}{\partial x}\left(\frac{1}{3}\frac{\partial^2 P}{\partial x\partial t}+\frac{1}{6}\frac{\partial^2 Q}{\partial y\partial t}+2Bgh\frac{\partial^2 \eta}{\partial x^2}+Bgh\frac{\partial^2 \eta}{\partial y^2}\right)\end{array}\right]\end{aligned} \tag{3}$$

$$\frac{\partial Q}{\partial t}+gD\frac{\partial \eta}{\partial y}+\varepsilon\left[\frac{\partial}{\partial x}\left(\frac{P^2}{D}Q\right)+\frac{\partial}{\partial y}\left(\frac{Q^2}{D}\right)\right]$$
$$=\mu^2\left[\begin{array}{l}\left(B+\frac{1}{3}\right)h^2\left(\frac{\partial^3 P}{\partial x\partial y\partial t}+\frac{\partial^3 Q}{\partial y^2\partial t}\right)+Bgh^3\left(\frac{\partial^3\eta}{\partial x^2\partial y}+\frac{\partial^3\eta}{\partial y^3}\right)\\ +h\frac{\partial h}{\partial x}\left(\frac{1}{6}\frac{\partial^2 P}{\partial y\partial t}+Bgh\frac{\partial^2\eta}{\partial x\partial y}\right)+h\frac{\partial h}{\partial y}\left(\frac{1}{6}\frac{\partial^2 P}{\partial x\partial t}+\frac{1}{3}\frac{\partial^2 Q}{\partial y\partial t}+Bgh\frac{\partial^2\eta}{\partial x^2}+2Bgh\frac{\partial^2\eta}{\partial y^2}\right)\end{array}\right] \quad (4)$$

where η is the instantaneous water surface elevation. P and Q are the depth-integrated velocity components (flux per unit width) in the x and y direction, respectively. h is the still water depth and D ($=h+\eta$) is the total water depth. g is the gravitational acceleration. ε and μ are the small parameters normalized by wave number k which indicate the nonlinear effects (ak) and dispersion effects (kh), respectively, where a is the wave amplitude. The governing equations take into account up to $O(\varepsilon)$ for nonlinearity and $O(\mu^2)$ for dispersion. The parameter B is the dispersion enhancement coefficient. For B = 1/15, the weak-nonlinear wave shoaling and wave dispersion closely correspond to the linear wave theory (Madsen and Sørensen, 1992). The further improvements of the Boussinesq model (*e.g.* wave breaking, runup and wave overtopping models) have been conducted to accurate estimation of wave transformations for engineering application in coastal and harbor zones (*e.g.* Hirayama, 2013b).

The governing equations is discretized by the ADI (Alternating Direction Implicit) method with the staggered grid, and the second-order central difference method and the Euler explicit method are applied to the spatial and temporal derivative terms, respectively.

2.2 Outline of numerical simulations and experiments

The numerical simulations using the Boussinesq model were performed to understand the aftereffects of the third-order nonlinear interactions from deep to shallow water region in comparison with a series experiments by Kashima et al. (2012). In the original experiments, the eight different wave condition changing values of spectral bandwidth and wave steepness have been investigated in five different bathymetries. In this paper, we will consider the only most particular case (*i.e.*, the most strong nonlinear case), which corresponds to a JONSWAP-type spectrum with γ_i = 10 and wave steepness, H_i/L_p of 0.04 for two different bottom bathymetry as shown in Figure 1. Here H_i is incident significant wave height and L_p is wave length for deep-water wave with peak frequency, f_p = 1.0 Hz, which gives the spectral peak wave

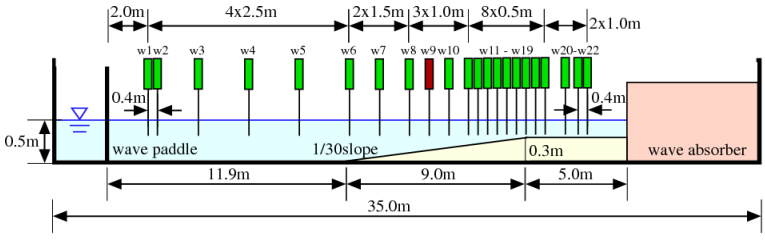

(a) Bathymetry type 1

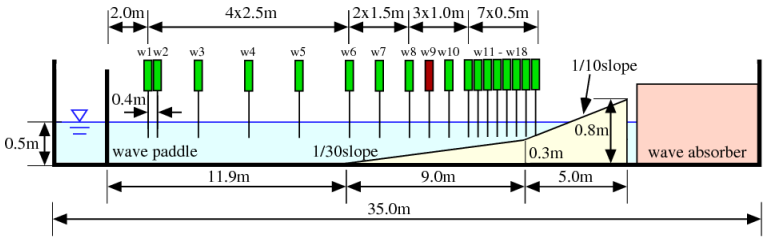

(b) Bathymetry type 2

Figure 1. Cross sectional view of bathymetry configurations.

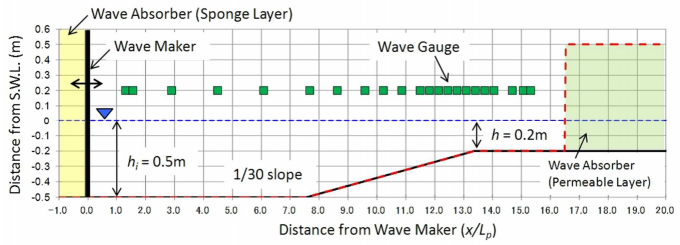

(a) Case: Input signal

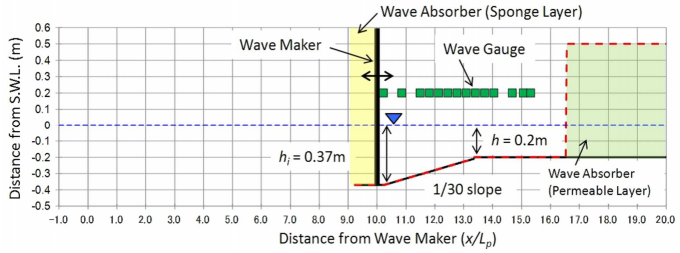

(b) Case: Measurement signal

Figure 2. Numerical setup for bathymetry type 1.

number k_p = 4.03 m^{-1}. The bathymetry type 1 has a impermeable 1/30 slope installed with the toe 11.9 m from the wave maker and a flat ground bottom, of which constant water depth is equal to 0.2 m. In the bathymetry type 2, the two different slopes are installed at the toe 11.9 m from the wave maker and the water depth at the inflection point of them is equal to 0.2 m. Each water depth in front of the wave maker for the bathymetry type 1 and 2 is same to 0.5 m.

In the numerical simulations, the two set of input water surface elevations were selected to investigate the effects of the third-order nonlinear interactions. One is the water surface elevation which corresponds to the initial wave signal given to the wave maker in the original experiments which initial wave profile is basically linear (Figure 2 (a)). The other case is the water surface elevation measured at the leading edge of slope (measurement point 12.5 m from the wave maker) as shown by the red wave gauge on Figure 1 which measured profile is influenced by full nonlinear interaction during the propagation on flat bottom, naturally (Figure 2 (b)). Hereafter, we will call these input wave surface elevations as 'input signal' and 'measurement signal', respectively. In particular, the latter signal includes the remarkable effects of the third-order nonlinear interactions in the deep water region.

The numerical domains for each wave signal were setup as shown in Figure 2. The each wave signal was generated at the leftward boundary and propagated to the right, and their initial water depth for each wave signal are h_i = 0.5 m and 0.37 m, respectively. The sponge layer 1.0L_p long was installed at the leftward boundary corresponding to the wave maker and the permeable layer 5.5 m long was installed at the rightward boundary corresponding to the wave absorber. The computational spatial and temporal resolutions were setup dx = 0.05 m and dt = 0.001 s to get high accuracy results of the numerical simulations, respectively.

As mentioned in the previous section, the probability density function of the maximum wave height depends on the number of waves in wave trains as shown in Eq. (1). Hence the long time numerical simulations are important to verify the effects of number of waves for understanding the maximum wave height, correctly. However, the long time numerical simulations have numerical errors during one calculation. Therefore ten calculation sets with the different random phases for input wave spectra were performed as well as the wave generation method of the original experiments. The total number of individual waves was about 10,000 waves defined by zero-down crossing from ten calculation sets.

In our analysis, the 50 wave trains are extracted from 10,000 wave data sets, assuming the number of wave heights for one wave train is defined as N = 200. The wave statistics such as skewness, kurtosis and maximum wave height are analyzed for 50 wave trains. Skewness and kurtosis which indicate the wave nonlinearity are defined as:

$$\mu_3 = \frac{1}{\eta_{rms}^3} \cdot \frac{1}{n} \sum_{i=1}^{n} \left(\eta_i - \eta_m \right)^3 \tag{5}$$

$$\mu_4 = \frac{1}{\eta_{rms}^4} \cdot \frac{1}{n} \sum_{i=1}^{n} (\eta_i - \eta_m)^4 \tag{6}$$

where η_i is the water surface elevation, η_m is the averaged value of η_i, η_{rms} is the root mean square value of η_i, and n is the number of data point. From Eqs. (5) and (6), the linear random waves correspond to $\mu_3 = 0$ and $\mu_4 = 3$, respectively.

3. Results and discussion

3.1. *Nonlinear property of the Boussinesq model*

First, the basic nonlinear properties using the Boussinesq model were investigated through the comparison with the experiments. Figure 3 shows the spatial developments of both skewness and kurtosis

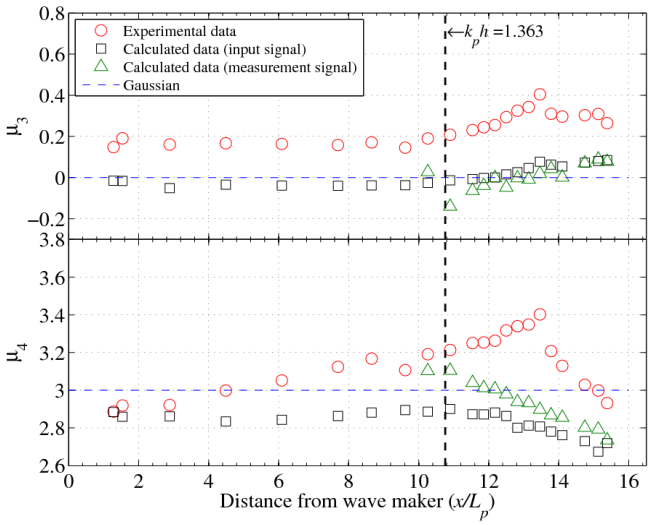

(a) Bathymetry type 1

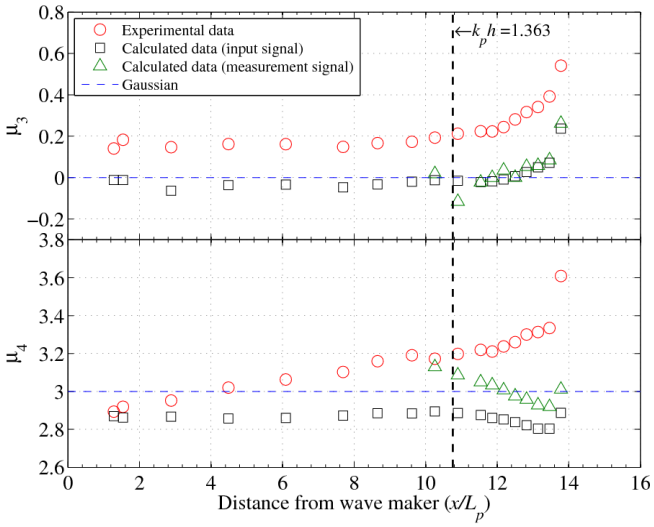

(b) Bathymetry type 2

Figure 3. Spatial distributions of skewness and kurtosis simulated using the Boussinesq model for the bathymetry type 1 and 2. (circle: experimental data, square: simulated data for input signal, triangle: simulated data for measurement signal, shin dashed line: Gaussian distribution)

of the surface elevation on the two different bottom bathymetries for the case of $\gamma_i = 10$ and $H_i/L_p = 0.04$. The horizontal axis is the dimensionless distance from the wave maker x/L_p and the vertical axes are the skewness and kurtosis given as the average values of 50 wave trains, respectively. The circles are the experimental data and the squares and triangles are the simulated data for input and measurement signals, respectively. The shin dashed line indicates by the Gaussian distribution. The vertical solid dashed bars indicate the line of $k_ph = 1.363$. For the bathymetry type 1, the spatial development of the skewness as shown in the experimental results, which depends on the wave steepness following the second-order nonlinear theory by Longuet-Higgins (1963), cannot be seen in the simulated data of $k_ph > 1.363$ ($x/L_p < 10.76$) for input signal. For this reason, the nonlinear interactions given by the Boussinesq model are expressed by the balance of the nonlinear term of $O(\varepsilon)$ and the dispersion term of $O(\mu^2)$. However, although the simulated skewness are slightly increased by wave shoaling under the effect of the bottom bathymetry when k_ph becomes smaller than 1.363 ($x/L_p > 10.76$), they remain less than one fifth of the experimental data. On the other hand, the simulated kurtosis of $k_ph > 1.363$ for input signal cannot show appropriately the spatial developments. The kurtosis evolution by the experimental data in deep water region caused by quasi-resonant four-wave interactions at the order of $O(\varepsilon^3)$ but such high-order nonlinear interactions of more than $O(\varepsilon,\mu^2)$ are not considered in the momentum equation of the Boussinesq model. Even in the shallow water region of $k_ph < 1.363$ ($x/L_p > 10.76$), the Boussinesq model significantly underestimates the nonlinear properties related to the freak wave occurrence. On the contrary, the results of both skewness and kurtosis in the numerical simulations for measurement signal show a similar tendency to the ones for input signal. For the bathymetry type 2, the differences between the experimental and simulated data for both wave signals are quite similar to the ones for the bathymetry type 1, except for the data on the 1/10 steep slope.

Figure 4 shows the relationship between the skewness and kurtosis for the bathymetry type 1 and 2. The horizontal and vertical axes are skewness and kurtosis, respectively. The legend of markers is same to Figure 3 but the opened and filled marks are the data of $k_ph > 1.363$ and $k_ph < 1.363$, respectively. The solid line is the second-order nonlinear theory in consideration of the water depth changing (Mori and Kobayashi, 1998) and the dashed-dotted line is the empirical equation introduced by the field data in the beach with 1.4 to 24.4 m water depth (Ochi and Wang, 1984). Both theoretical and empirical equations mean that the skewness developed by second-order nonlinear interactions associated with wave shoaling effects on the kurtosis change when the behaviors of the skewness and kurtosis obey these second order relations, although the skewness and kurtosis are independent for the four wave interactions. For the wave propagations over the slope of the bathymetry type 1, the development of kurtosis for the experimental results is mixed by the second and third order nonlinear interactions. The third-order nonlinearity under the effects of quasi-resonant four-wave interactions changed kurtosis but kept skewness constant in the deep water region of $k_ph > 1.363$. After that the second-order nonlinearity changed skewness due to wave shoaling on the slope in the shallow water region of $k_ph < 1.363$. The changes of kurtosis caused by the second- nonlinearity through skewness change in the shallow water. However, in the Boussinesq model for not only input but also measurement signal, the behaviors of the skewness and kurtosis related to k_ph changing completely differs from the ones of the experiments. In addition, for the bathymetry type 2 there is also no correlative relationship between the skewness and kurtosis of the simulated data as well as the ones for the bathymetry type 1.

Thus, these results imply that the standard Boussinesq model may not appropriately evaluate the freak wave occurrence caused by the developments of the third-order nonlinear interactions propagating from deep to shallow water region. Therefore, it is necessary to correct the insufficient nonlinearity of the numerical simulations to describe the extreme wave occurrence in the shallow water region using the Boussinesq model.

3.2. *Correction of nonlinear effect*

In the previous section, we have investigated the significant differences of the nonlinear properties such as the development processes of skewness and kurtosis between the numerical simulations using the Boussinesq model and the original experiments for the bathymetry type 1 and 2. However, we cannot predict the freak wave occurrence correctly in the shallow water region using the Boussinesq model data unless solving the above mentioned insufficient nonlinearity. The nonlinearity of more than $O(\varepsilon^2)$ which cannot be expressed in the Boussinesq model is going to be corrected analytically in this section.

First, the corrected skewness μ_3' was given by Eq. (7) considering the difference between the data of the

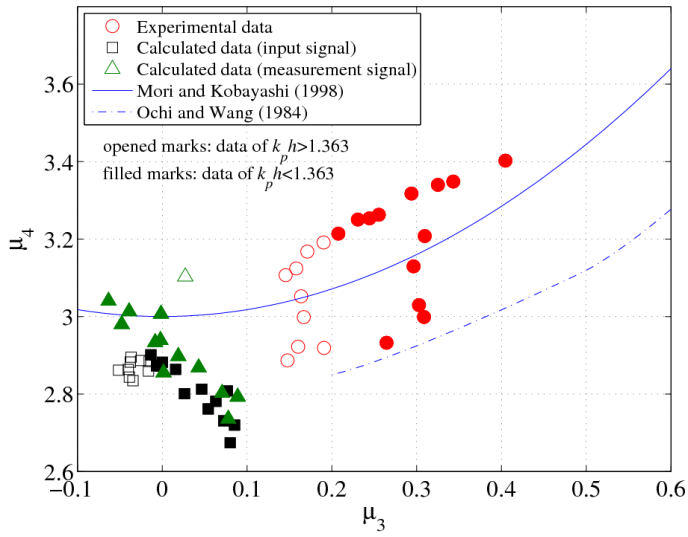

(a) Bathymetry type 1

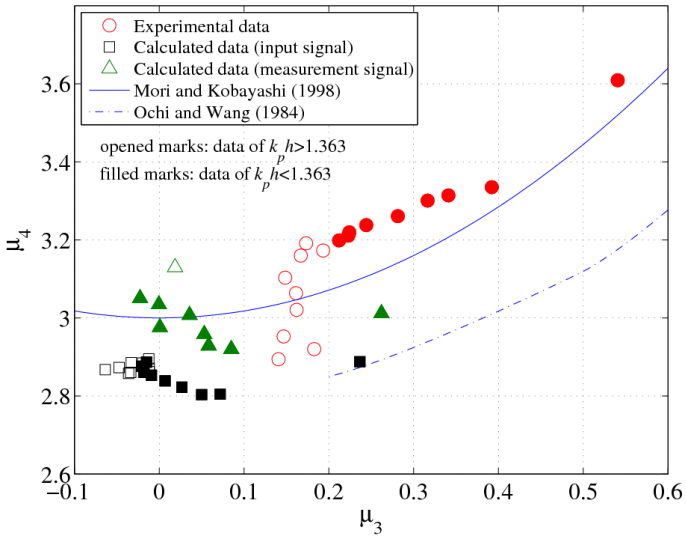

(b) Bathymetry type 2

Figure 4. Relationship between skewness and kurtosis. (circle: experimental data, square: simulated data for input signal, triangle: simulated data for measurement signal, opened marks: the data of k_ph > 1.363, filled marks: the data of k_ph < 1.363, solid line: second-order nonlinear random theory by Mori and Kobayashi (1998), dashed line: the empirical equation by Ochi and Wang (1984))

numerical simulations and experiments in the deep water region of k_ph > 1.363.

$$\mu_3^{'} = \mu_3^{(2)} + \mu_3^{cal} \tag{7}$$

where μ_3^{cal} is the skewness given by the Boussinesq model for input signal. $\mu_3^{(2)}$ is the skewness expressed by the second-order nonlinear theory of Longuet-Higgins (1963) and is given by

$$\mu_3^{(2)} = 3k_p\sqrt{m_0} \tag{8}$$

where m_0 is the zero-order moment corresponding to the dispersion of the water surface elevation.

Next, the corrections of kurtosis in the deep water region of k_ph > 1.363 was conducted by using the

spatial development process under the effects of the third-order nonlinear interactions from the experimental data. Eq. (9) is simply introduced by the spatial development of kurtosis in the deep water region from the experimental data for the case of γ_i = 10 and H_i/L_p = 0.04.

$$\mu_4^{(3)} = \left(\mu_4^{cal}\right)_0 + 0.0184\left(x / L_p\right) \tag{9}$$

where $\mu_4^{(3)}$ and $(\mu_4^{cal})_0$ are the corrected kurtosis in the deep water region and the kurtosis given immediately after wave generation, respectively.

Following the above mentioned developments of skewness and kurtosis in the deep water region of k_ph > 1.363 given by Eqs. (7) and (9), the corrected kurtosis in the shallow water region of k_ph < 1.363, μ_4' can be obtained by using the relational expression between skewness and kurtosis (*i.e.*, Mori and Kobayashi, 1998) which is approximated by the Gaussian combination of the Stokes waves in the shallow water region;

$$\mu_4' = \mu_4^{(3)} + \left(\frac{4}{3}\right)^2 \mu_3' \tag{10}$$

Figure 5 shows the spatial developments of the skewness and kurtosis for the same condition in Figure 3 by the above correction method. The circles and squares are the experimental data and simulated data for input signal, respectively. The filled diamonds are the simulated data corrected by Eqs. (7)-(10). Although there is a slight difference between the simulated data with the corrections and experimental data on the 1/30 slope of k_ph < 1.363, the simulated data with the corrections seems to describe an good agreement with the results of the experiments. Thus, the behaviors of both skewness and kurtosis related to the freak wave occurrence in the shallow water region can be estimated by the analytical corrections of the high-order nonlinearity of more than $O(\varepsilon^2)$ to the Boussinesq model simulation, approximately.

4. Conclusion

In this study, a series of numerical simulations by using the Boussinesq model were conducted to investigate the aftereffects of the third-order nonlinear interactions from deep to shallow water region related to freak wave occurrence. Although the Boussinesq model cannot express the higher-order nonlinear interactions of more than $O(\varepsilon^2)$, the aftereffects of the offshore freak waves shoaling to coasts can be expressed by the analytical corrections of the nonlinear properties (*i.e.*, developments of skewness and kurtosis from deep to shallow water region).

Further detail simulation and analyses using this nonlinear correction will be required to understand the freak wave occurrence (*i.e.*, the probability density function of maximum wave height) using the standard Boussinesq model. The difference between the standard Boussinesq model and full nonlinear Boussinesq model for extreme prediction remains future study.

Acknowledgements

This research was partially supported by the Ministry of Education, Science, Sports and Culture, Japan, though Grant-in-Aid (PI: Nobuhito Mori).

References

Hirayama, K., 2002. Utilization of numerical simulation on nonlinear irregular wave for port and harbor design. *Technical Note of The Port and Airport Research Institute*, 1036: 162 (in Japanese).

Hirayama, K., 2013a. Harbor tranquility analysis method for using Boussinesq-type nonlinear wave transformation model. *Proceedings of 23rd International Offshore and Polar Engineering Conference, Rhodes, Greece*. (in press).

Hirayama, K., 2013b. Numerical simulations using Boussinesq model for random sea wave transformations. *11th International Workshop on Coastal Disaster Prevention*.

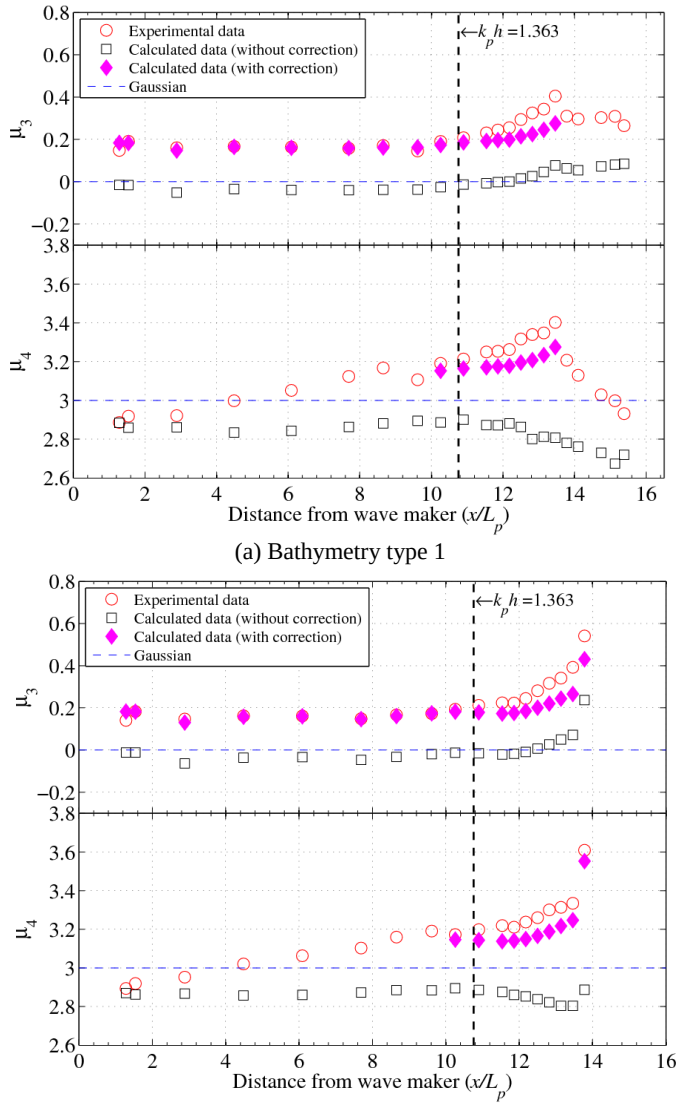

(a) Bathymetry type 1

(b) Bathymetry type 2

Figure 5. Spatial distributions of skewness and kurtosis after correction of nonlinearity. (circle: experimental data, square: simulated data with no correction, diamond: simulated data with correction, dashed line: Gaussian distribution)

Janssen, P.A.E.M., 2003. Nonlinear four-wave interactions and freak waves. *Journal of Physical Oceanography.*, 33(4): 863-884.

Janssen, P.A.E.M. and M. Onorato, 2007. The intermediate water depth limit of the Zakharov equation and consequences for wave prediction. *Journal of Physical Oceanography*, 37(10): 2389-2400.

Kashima, H., K. Hirayama and N. Mori, 2012. Shallow water effects on freak wave occurrence. *Proceedings of 22nd International Offshore and Polar Engineering Conference, Rhodes, Greece*, 3: 778-783.

Longuet-Higgins, M., 1963. The effect on non-linearities on statistical distributions in the theory of sea waves. *Journal of Fluid Mechanics*, 17: 459-480.

Madsen, P.A. and O.R. Sørensen, 1992. A new form of the Boussinesq equations with improved linear dispersion characteristics. Part2. A slowly-varying bathymetry. *Coastal Engineering*, 18: 183-204.

Mori, N. and N. Kobayashi, 1998. Nonlinear distribution of nearshore free surface and velocity. *Proceedings of 26th International Conference of Coastal Engineering*, 1: 189-202.

Mori, N. and P.A.E.M. Janssen, 2006. On kurtosis and occurrence probability of freak waves. *Journal of Physical Oceanography*, 36(7): 1471-1483.

Mori, N., M. Onorato, P.A.E.M. Janssen, A.R. Osborne and M. Serio, 2007. On the extreme statistics of long-crested deep water waves: Theory and experiments. *Journal of Geophysical Research*, 112, C09011,

doi:10.1029/2006JC004024.
Mori, N., M. Onorato and P.A.E.M. Janssen, 2008. Directional effects on freak wave prediction. *Proceedings of 31st International Conference of Coastal Engineering*, 1: 392-403.
Mori, N., M. Onorato and P.A.E.M. Janssen, 2011. On the estimation of the kurtosis in directional sea states for freak wave forecasting. *Journal of Physical Oceanography*, 41(8): 1484-1497.
Ochi, M. and W.C. Wang, 1984. Non-Gaussian characteristics of coastal waves. *Proceedings of 19th International Conference of Coastal Engineering*, 1: 516-531.
Petrova, P., and C. Guedes Soares, 2008. Maximum wave crest and height statistics of irregular and abnormal waves in an offshore basin, *Applied Ocean Research*, 30, 144-152.
Trulsen, K., H. Zeng and O. Gramstad, 2012. Laboratory evidence of freak waves provoked by non-uniform bathymetry. *Physics of Fluids*, 24, 097101.
Waseda, T., T. Kinoshita, and H. Tamura, 2009. Evolution of a random directional wave and freak wave occurrence. *Journal of Physical Oceanography*, 39, 621–639.
Xiao, W., Y. Liu, G. Wu, and D. K. Yue , 2013. Rogue wave occurrence and dynamics by direct simulations of nonlinear wave-field evolution. *Journal of Fluid Mechanics*, 720, 357-392.
Yasuda, T. and N. Mori, 1993. High order nonlinear effects on deep-water random wave trains. *International Symposium: Waves-Physical and Numerical Modelling, Vancouver*, 2: 823-832.
Yuen, H. and B.M. Lake, 1982. Nonlinear dynamics of deep-water gravity waves. *Advances in Applied Mechanics*, 22: 67-327.
Zeng, H and K. Trulsen, 2012. Evolution of skewness and kurtosis of weakly nonlinear unidirectional waves over a sloping bottom. *Natural Hazards and Earth System Sciences*, 12: 631-638.